Parallel energy analyzer for pure electron plasma devices

D. L. Eggleston
Occidental College, Los Angeles, California 90041

C. F. Driscoll, B. R. Beck, A. W. Hyatt, and J. H. Malmberg
University of California at San Diego, La Jolla, California 92093

(Received 30 April 1992; accepted 29 June 1992)

A technique is presented for measuring the parallel energy distribution of magnetically confined electrons in a cylindrically symmetric pure electron plasma. In essence, the technique measures how many electrons are energetic enough to escape past applied confinement potentials. The technique does not require any secondary magnetic fields. Simplified variations of the technique are also presented which can be used at the expense of some loss of information. These techniques have been successfully used in three experimental contexts.

I. INTRODUCTION

Single species plasmas have been studied for some time, both experimentally and theoretically.[1] Much of the recent experimental work has been performed on pure electron plasma devices with cylindrical geometry.[2,3] Radial confinement of the plasma is provided by an axial magnetic field, and axial confinement is provided by electrostatic end potentials. The devices are typically run in cycles, with the electrons being axially dumped at the end of each cycle. By measuring the dumped electrons with a radially movable collector, one can determine the density profile of the plasma. This density data provided the basis for much of the early work on these devices.

However, a detailed understanding of these plasmas often requires a knowledge of the temperature or distribution function of electrons moving parallel to the axial magnetic field. Two major problems arise when developing a diagnostic for these quantities: First, the analysis of the dumped electrons is complicated by the fact that the electrostatic potential energy in a pure electron plasma is always much greater than the average electron kinetic energy kT. This means that when the electrons are dumped their energy is largely determined by the plasma potential, rather than by the details of the original distribution function. Additionally, the diagnostic development is constrained by the need to maintain cylindrical symmetry to avoid degrading plasma confinement.

In this paper we present a technique for measuring the parallel energy distribution function, giving $T_\parallel(r)$. Essentially, we measure how many electrons can escape past various applied confinement potentials. A computer-assisted analysis of collected charge taken as a function of both radius and confinement potential allows us to remove plasma potential effects and extract the desired distribution function. Cylindrical symmetry is maintained by employing existing cylindrical electrodes to apply the analyzer potentials. We also present simplified variations of the technique for special applications. These techniques have been successfully used on three different experiments.

II. EXPERIMENTAL DEVICE

The cylindrical electrodes of a typical pure electron plasma device are shown schematically in Fig. 1(a). The electrodes are immersed in a uniform axial magnetic field B and a vacuum of 10^{-10} Torr. The cylindrical conducting wall is divided into rings of various lengths. The injection and containment rings G1 and G3 are normally held at large negative voltages, and the remaining rings are usually grounded. The machine operation normally follows an inject-hold-dump cycle, shown in Fig. 1(b). To start a cycle, ring G1 is switched to ground potential, allowing electrons from a negatively biased spiral filament to fill the region between the filament and G3. Ring G1 is then returned to a negative potential, trapping the electron column. While the plasma is confined, the various rings between G1 and G3 can be used to monitor wave activity in the plasma or to apply electric fields to the plasma.

After a variable time, the electrons are dumped by grounding ring G3. The electrons move along magnetic field lines and are collected either by a radially movable probe (giving the z-integrated density at a particular radius) or by a plate (giving the total number of electrons in the device). Typical parameters are electron density $n \simeq 10^7$ cm^{-3}, electron thermal energy $kT \simeq 1$ eV, plasma radius $R_p \sim 1$ cm, and axial magnetic field $B = 40$–675 G. However, these parameters can vary significantly in different devices. For example,[4,5] in a device with a superconducting 80 kG magnet, $n \lesssim 10^{10}$ cm^{-3}, 0.001 eV$\leqslant kT \leqslant$200 eV, and $R_p \sim 0.1$ cm.

Much of the utility of these devices stems from their extremely long confinement times.[6] This feature makes these devices especially suitable for controlled studies of cross-field transport, since the background transport is small. The confinement of electrons in currently operating devices (with neutral pressure $P_n < 10^{-7}$ Torr) appears to be limited by small electric or magnetic field asymmetries associated with construction imperfections. These background field errors cause electrons to drift radially and be lost to the wall. When care is taken to avoid construction asymmetries, the confinement improves.[6] When additional asymmetries are deliberately applied to the plasma, additional radial transport is observed.[7] Field asymmetries and asymmetric resistive walls have also been shown to affect the stability of these plasmas.[8,9] It is thus highly desirable to maintain cylindrical symmetry in the design of these devices.

 0899-8213/92/103432-08$04.00

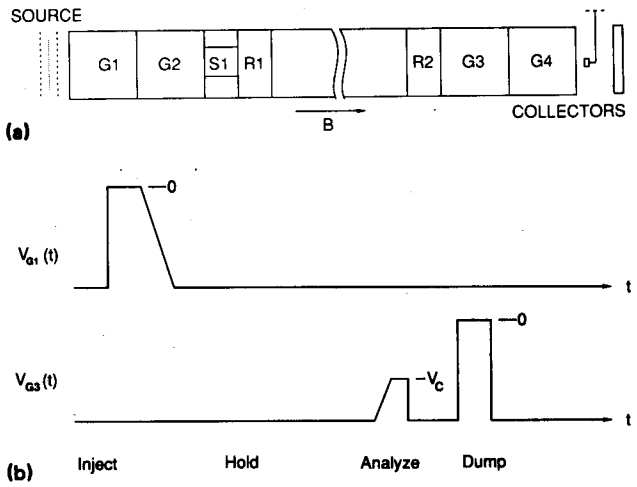

FIG. 1. Experimental device and timing sequence. (a) Schematic of containment electrodes. The plasma is confined between cylinders G1 and G3. (b) Experimental timing sequence for $V_{G1}(t)$ and $V_{G3}(t)$. The voltage applied to G3 has both an analysis pulse and a dump pulse.

The desire to maintain cylindrical symmetry and avoid perturbing fields has, in practice, limited the diagnostics on these machines. As mentioned above, the plasma density can be obtained by collecting electrons dumped at the end of each machine cycle. One may also pass the dumped electrons through a spatially varying magnetic field prior to collection, to obtain information on the average energy $kT_\perp$ of the electron motion perpendicular to the magnetic field. This is sometimes referred to as a magnetic beach analyzer.[3,10,11] While this technique is useful, it does require the addition of an analyzing magnetic field to the device. Since the energy distributions of electrons moving perpendicular and parallel to the magnetic field lines are not necessarily the same, the $T_\perp$ measurement is complementary to the $T_\parallel$ measurement described here.

The rings within the confinement volume may be used to launch and detect plasma waves and also to measure the total charge per unit length of the plasma column.[2,3,7–9] Typically, some of the rings [e.g., ring S1 in Fig. 1(a)] are divided azimuthally into sectors, to enable launching and detecting waves with nonzero azimuthal mode number. This wave data can give some indication of the parallel electron temperature via parameter fits to the electron plasma wave dispersion curves.[8,12] However, this technique gives a weighted radial average of $T_\parallel$ which is not generally sufficient for detailed comparisons between theory and experiment.

Attempts to obtain information about the parallel velocity distribution from the dumped electrons are complicated by the large plasma potential $\phi_p(r)$ characteristic of non-neutral plasmas. For example, it is easy to show that for a pure electron plasma column of radius R_p bounded by a grounded cylinder of radius R, $q\phi_p(0)/kT=(R_p^2/4\lambda_D^2)[1+2\ln(R/R_p)]$, where q is the electron charge and $\lambda_D\equiv(kT/4\pi nq^2)^{1/2}$ is the Debye length. Since experimentally interesting plasmas have $R_p/\lambda_D\gg1$, they also have $q\phi_p(0)\gg kT$. When an electron is dumped, it will increase its parallel energy by approximately $q\phi_p$. Since this energy is large compared to kT, varies with radius and time, and depends on the radial density profile, one might expect that extracting information about the electron's original parallel energy would be a hopeless task. However, with the data collection and analysis techniques presented here, one can in fact obtain most of the original parallel electron energy distribution at all radii. Further, the technique does not require modification of typical machine geometries.

III. DESCRIPTION OF THE DIAGNOSTIC AND ANALYSIS MODEL

To measure the electron density, all of the electrons in the machine are dumped and collected at the end of a machine cycle, by switching the confinement voltage on ring G3 to ground. To measure the parallel energy distribution, we measure the number of electrons which escape past a lowered, but nonzero, confinement potential. In practice, this requires a two-step dump, as shown in Fig. 1(b). First, the confining voltage on G3 is switched to a selected value V_c. This allows electrons with parallel kinetic energy exceeding some value to escape and be collected on the radially movable collector, giving a measured charge Q_{esc}. The remaining electrons are dumped shortly afterwards to prepare for a new machine cycle. The value of V_c is changed slightly on subsequent machine cycles, giving $Q_{esc}(V_c)$. This procedure is repeated with the collector at several radial positions from $r=0$ to the cylinder wall at $r=R$. A complete raw data set thus gives us the function $Q_{esc}(r,V_c)$.

We note that applying a voltage V_c to G3 gives a confinement potential ϕ_c which is somewhat less than V_c due to the finite length of G3. The raw data needs to be corrected to account for this. For a given applied voltage V_c the confinement potential ϕ_c will vary with radius r. The map from the set of V_c values to a set of ϕ_c values will also therefore depend on radius. However, later on in the data analysis we will need to know how Q_{esc} varies with r for a constant value of ϕ_c. Thus after the radially dependent map $V_c\rightarrow\phi_c$ has been applied to the data, we interpolate between the Q_{esc} and ϕ_c values so that, at each radius, we have Q_{esc} values at the *same* set of confinement potentials ϕ_c. With these corrections, we obtain our basic data set of $Q_{esc}(r,\phi_c)$.

We now discuss how the parallel energy distribution function $F(r,E)$ can be obtained from the $Q_{esc}(r,\phi_c)$ data. A discussion of the assumptions inherent in this analysis is given in Sec. VI. Consider a cylindrically symmetric electron column of length L and electron density $n(r)$ before any charge escapes. With the radial collector centered at radius r, the charge it collects for a given ϕ_c is

$$Q_{esc}(r,\phi_c)=qL\int dA'n(r')\int_E^\infty\frac{dE'}{\sqrt{E'}}F(r',E'),\qquad(1)$$

where $\int dA'$ is an integral over the collector area which is centered at r. Here, $F(r,E)$ is the parallel velocity distribution function f, written in terms of energy; i.e., $F(r,\frac{1}{2}mv_\parallel^2)=f(r,v_\parallel)\sqrt{2/m}$. The number of particles be-

tween E and $E+dE$ is therefore $E^{-1/2}F(E)dE$, and $\int_0^\infty (dE/\sqrt{E})F(E) = 1$. For the second integral in Eq. (1), the lower integration limit $E(r,\phi_c)$ is the minimal electron kinetic energy required to escape over the confining potential ϕ_c, and is given by

$$E(r,\phi_c)=q[\phi_c-\phi_p(r,\phi_c)], \tag{2}$$

where $\phi_p(r,\phi_c)$ is the plasma potential produced by the electrons that remain confined. The plasma potential ϕ_p and thus the electron kinetic energy E are evaluated at a plane midway along the axis, away from the end regions where the potential is varying with z.

When the collector size is sufficiently small Eq. (1) can be approximated as

$$Q_{\rm esc}(r,\phi_c)=Q(r)\int_E^\infty \frac{dE'}{\sqrt{E'}}F(r,E'), \tag{3}$$

where $Q(r)=qALn(r)$ and $A=\int dA'$ is the area of the collector. We shall assume a small collector size and employ Eq. (3) from here on. The plasma potential in Eq. (2) may be obtained from Poisson's equation:

$$\frac{1}{r}\frac{d}{dr}\left(r\frac{d}{dr}\phi_p(r,\phi_c)\right)=-4\pi qn(r)\left(1-\frac{Q_{\rm esc}(r,\phi_c)}{Q(r)}\right), \tag{4}$$

with boundary conditions $\phi_p(R,\phi_c)=0$ and $(d\phi_p/dr)(0,\phi_c)=0$.

By differentiating Eq. (3) with respect to E, we obtain the distribution function:

$$F(r,E)=-\sqrt{E}\frac{d}{dE}\left(\frac{Q_{\rm esc}}{Q}\right)$$

$$=-\sqrt{E}\left(1-\frac{d\phi_p}{d\phi_c}\right)^{-1}\frac{d}{dq\phi_c}\left(\frac{Q_{\rm esc}}{Q}\right). \tag{5}$$

To use the first form of Eq. (5), we need to know $Q_{\rm esc}$ as a function of E. The data set, however, gives us $Q_{\rm esc}$ as a function of the confining potential ϕ_c. We thus require a map of ϕ_c onto $E=q(\phi_c-\phi_p)$. Finding this map is the central difficulty in doing energy analysis for non-neutral plasmas. The necessity of this map stems from the fact that the analyzing potential in this situation is $\phi_c-\phi_p$, whereas the experimentally controlled potential is ϕ_c. The map can be obtained from the data set which gives us $Q_{\rm esc}$ as a function of r for each value of ϕ_c. These data allow us to numerically integrate Eq. (4) to obtain $\phi_p(r)$ for each ϕ_c. This in turn allows us to construct the required map of $\phi_c\rightarrow E$ for each r. The same information is required to use the second form of Eq. (5), which requires knowledge of $d\phi_p/d\phi_c$.

IV. RESULTS

The results of the analysis of some typical data are shown in Fig. 2. The data set consists of $Q_{\rm esc}$ measurements for 125 values of ϕ_c at each of 35 radial positions. Figure 2(a) shows $Q_{\rm esc}$ as a function of the experimentally varied potential energy $q\phi_c$ for three of the radial positions. Here, $Q_{\rm esc}(r,\phi_c)$ is normalized to $Q_0\equiv Q(r=0)=Q_{\rm esc}(r=0,\phi_c=0)$ and the radius r is normalized to the wall radius R. At the highest values of $q\phi_c$, all the electrons are confined. As ϕ_c approaches zero, more and more of the electrons have sufficient energy to escape and be collected.

This data set also gives $Q_{\rm esc}$ as a function of radius for any value of ϕ_c. With these data we can determine the amount of charge left in the machine, $Q_{\rm left}(r,\phi_c)\equiv Q(r)-Q_{\rm esc}(r,\phi_c)$, as a function of radius, and thus we can calculate ϕ_p from Eq. (4). Figure 2(b) shows plots of $Q_{\rm left}/Q_0$ for three representative values of $q\phi_c$. When the data for a particular value of ϕ_c is integrated radially, we obtain the plasma potential ϕ_p as a function of radius [Fig. 2(c)]. If this procedure is carried out for all values of ϕ_c, we obtain $\phi_p(r,\phi_c)$. This determines the required map of $\phi_c\rightarrow E$. In Fig. 2(d), we plot ϕ_p vs ϕ_c for three radii.

At this point we may plot $Q_{\rm esc}$ as a function of E. This is shown in Fig. 2(e). The parallel energy distribution function, $F(E)$, is then obtained by employing Eq. (5). For display purposes (i.e., to keep the normalization consistent with the other figures) we multiply F by Q/Q_0 and plot $\ln(FQ/Q_0)$ vs E in Fig. 2(f). For energies $E>1$ eV, the curves are roughly straight lines, indicating a near-Maxwellian distribution of energies; i.e., $F\propto\exp(-E/kT_\parallel)$. Fitting straight lines to these curves then gives $T_\parallel(r)$. The reasons for the failure of the technique at low energies are discussed in Sec. VI.

An example of $T_\parallel(r)$ obtained in this way is shown in Fig. 3, along with the measured density profile $n(r)$. As is typical for these electron plasmas, the temperature is seen to be low in the center and to rise near the edge. We have normalized the curves by their maximum values. Central ($r=0$) values are $n_0=5.66\times10^6$ cm^{-3} and $T_m=0.46$ eV.

These normalization values agree closely with values obtained from wave dispersion data. The dispersion curve of the azimuthally symmetric electron plasma wave (i.e., Trivelpiece–Gould[13] wave) is obtained by observing the frequencies of standing waves in the plasma column. A short tone burst is applied to ring R1 and a receiver is connected to ring R2. As the tone-burst frequency is slowly swept, peaks in the received signal indicate the standing wave frequencies. For a column of length L, the standing waves occur at wave numbers $k=n\pi/L$, where $n=1,2,3\ldots$. From this information, we can construct the dispersion curve.

The standing wave frequencies for a Maxwellian plasma column with arbitrary density and parallel temperature profiles can be obtained theoretically by numerically solving an eigenvalue equation.[14] If the normalized density and temperature profiles are known, the absolute density and temperature may be adjusted to obtain a best fit to the experimental dispersion curve. When the normalized density and temperature profiles of Fig. 3 are used, this method gives an absolute central density and temperature of $n_0=5.84\times10^6$ cm^{-3} and $T_m=0.45$ eV, respectively. These values agree well (within 3%) with the directly measured values. In contrast, if the same relative density profile were used but a flat temperature profile were assumed (i.e., one with no radial variation), a best fit to the dispersion data would give $n_0=7.68\times10^6$ cm^{-3} and

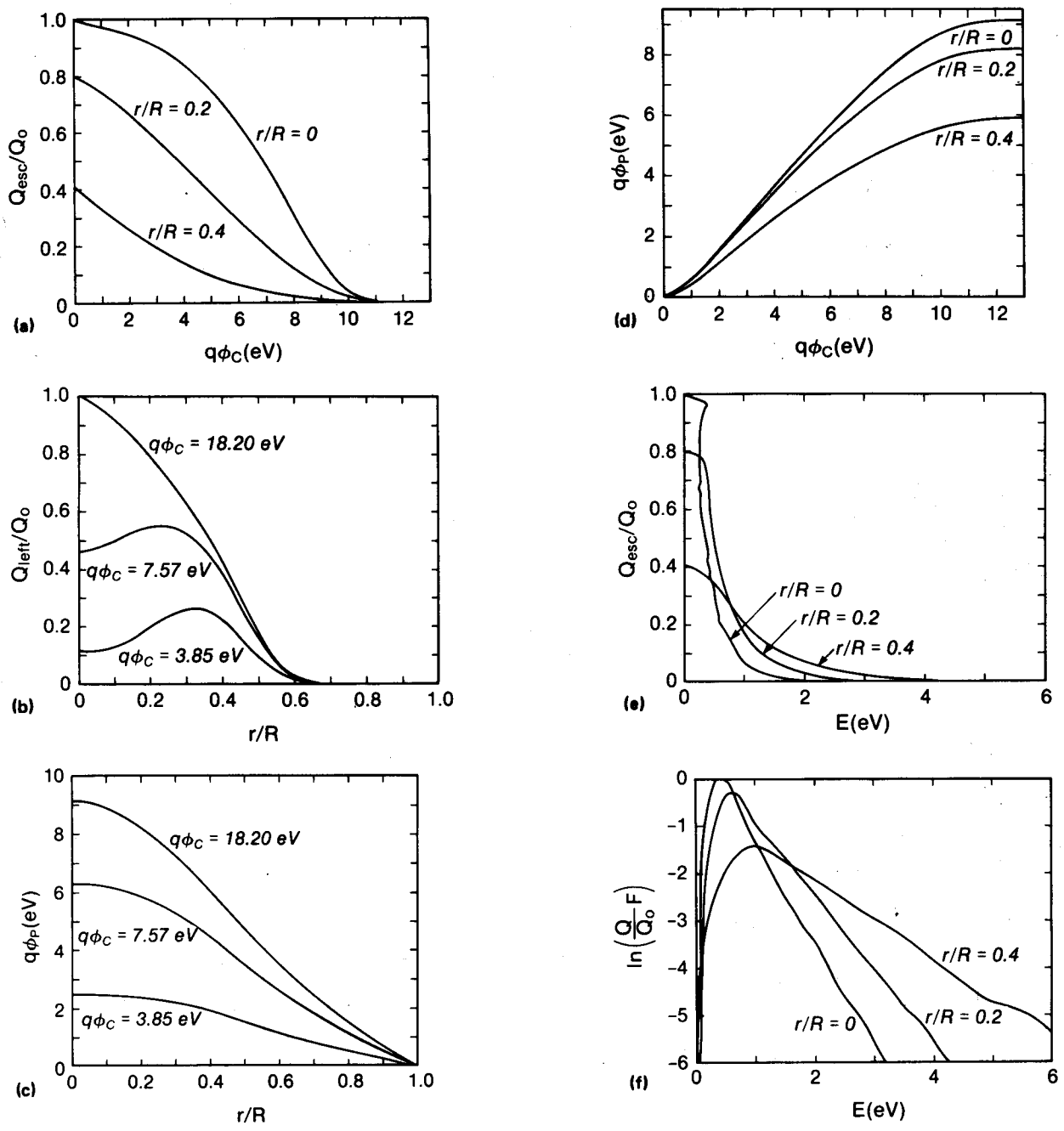

FIG. 2. Measured density data, and derived potentials and energies. (a) Measured escaping charge Q_{esc} versus applied confinement potential ϕ_c at several radii. Q_{esc} is normalized to $Q_0=Q_{esc}(r=0,\phi_c=0)$. (b) Remaining charge versus the normalized radius, for several confinement potentials ϕ_c. (c) Plasma potential ϕ_p versus radius. ϕ_p is calculated from the data of (b), using Eq. (4). (d) Calculated plasma potential ϕ_p versus confinement potential ϕ_c. (e) Measured Q_{esc} as a function of calculated $E=q(\phi_c-\phi_p)$. (f) Resulting energy distribution function $F(E)$, normalized by Q/Q_0.

$T_m=0.58$. In this case, the agreement with the directly measured values would be poor. Thus the dispersion data corroborate the directly measured temperature profile.

V. VARIATIONS OF THE TECHNIQUE

As we stated above, the central difficulty in using this technique is obtaining the map $\phi_c \rightarrow E$, i.e., the relation between the (corrected) applied potential and the effective confinement barrier. We experimentally control the potential ϕ_c but the data are understood in terms of the confinement barrier $\phi_c-\phi_p$. Obtaining the map requires a large data set and generally necessitates the use of a computer. In many cases, it is desirable to have a simpler approach, even at the expense of some loss of information.

The simplified techniques we present here analyze only the first particles which escape from the center of the plasma. The plasma potential $\phi_p(r)$ is not changed significantly by the escape of these first particles, so $d\phi_p/d\phi_c \approx 0$. Then, Eq. (5) gives the tail of $F(r=0,E)$ from a measurement of $Q_{esc}(r=0,\phi_c)$ vs ϕ_c, with only the constant $\phi_p(r=0)$ needed to relate E to ϕ_c.

Even more simply, if we assume that the parallel en-

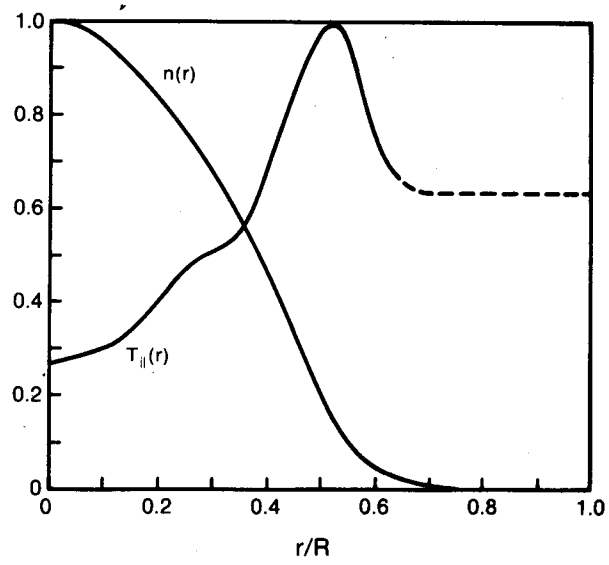

FIG. 3. Experimentally obtained density and parallel temperature profiles, normalized to their maximum values. The dashed portion of the temperature curve is unobtainable, but is specified to be flat for the parameter fit.

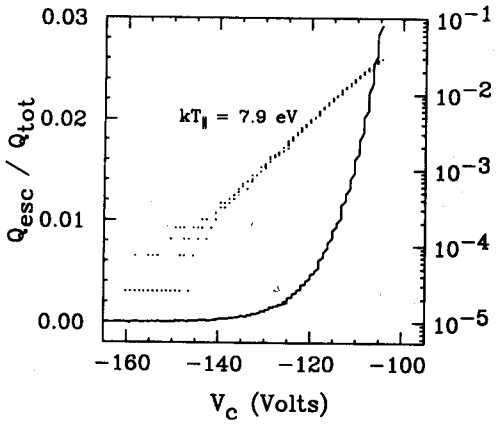

FIG. 4. Escaping charge Q_{esc}/Q_{tot} versus confinement voltage V_c on linear and logarithmic scales. Q_{tot} is the total charge initially trapped.

ergy distribution is Maxwellian; i.e.,

$$F(r,E)=(\pi kT_{\|})^{-1/2}\exp(-E/kT_{\|}), \tag{6}$$

then the second integral in Eq. (1) can be evaluated, and one obtains

$$Q_{esc}(r,\phi_c)=qL\int dA'\, n(r')\mathrm{erfc}\left(\sqrt{\frac{E(r',\phi_c)}{kT_{\|}}}\right), \tag{7}$$

where erfc is the complementary error function. When $E/kT_{\|}\gtrsim 2$, one finds from Eq. (7) that

$$\frac{d\ln(Q_{esc})}{d(q\phi_c)}=\frac{-1.05}{kT_{\|}} \tag{8}$$

to about 5% accuracy. Equation (8) does not assume a small collector size, except that the length scale for radial temperature variations must be small compared to the collector size.[4]

In addition to simplifying the data analysis, this technique also allows for a simplification in the way the data are obtained. Before we switched the confinement voltage on G3 to a value V_c and then measured Q_{esc} for that value. Here, we slowly ramp the confinement voltage toward ground and measure both Q_{esc} and V_c versus time with a transient digitizer. The required Q_{esc} vs V_c data can thus be obtained from a single machine cycle. Note that this method can only be used to obtain data on the first particles to escape from the plasma. The restrictions on ramp time discussed in Sec. VI prevent us from using the method with the bulk of the escaping particles.

Data obtained with this technique are shown in Fig. 4. We plot $Q_{esc}(r=0,\phi_c)/Q_{tot}$ vs V_c for $E/kT_{\|}\gg 1$, where $Q_{tot}=2\pi qL\int_0^R rn(r)dr$ is the total charge initially trapped. For this experiment, the confinement ring is long enough so that $\phi_c=V_c$ to good approximation (i.e., the confinement potential ϕ_c does not vary with radius as it does for shorter rings). The solid curve shows Q_{esc}/Q_{tot} increasing from zero as V_c approaches the plasma potential less a few $kT_{\|}$. The dotted curve shows the logarithm of Q_{esc}/Q_{tot}. The logarithmic data are essentially straight over about 2 decades, until so many charges have escaped that ϕ_p begins to change. The slope of the straight-line region gives $T_{\|}\approx 7.9$ eV from Eq. (8). At these high temperatures, it is relatively easy to obtain 2 or 3 decades of exponential signal. At temperatures below 10^{-2} eV, less than 1 decade may be obtained due to amplifier noise, and more sophisticated fitting techniques[4] are required to utilize the data inherent in the nonexponential region to obtain $T_{\|}$.

This simplified technique avoids the task of finding ϕ_p as a function of ϕ_c. However, since ϕ_p varies as electrons escape, only the tail of the distribution can be obtained before the change in ϕ_p becomes significant. Furthermore, the electrons which first escape come mostly from the region $r\lesssim 6\lambda_D$ since the parallel kinetic energy required to escape [see Eq. (2)] is smallest near the axis. Thus, the simplified technique can only measure the tail of the distribution near the axis (i.e., $v_{\|}\gg\bar{v}$ and $r\lesssim 6\lambda_D$). For some applications only $F(v_{\|})$ near the axis is required, and the simplification in the technique more than outweighs the loss of information. Also, the data are obtained from a single machine cycle. This single-shot temperature analysis is particularly useful when the "hold" portion of a machine cycle is very long, as it sometimes is in these experiments.

These simplified techniques have been employed successfully on two pure electron plasma apparatuses. The experiments involved the measurement of the equilibration of $T_{\|}$ and $T_{\perp}$ in a plasma after they were intentionally made unequal.[4,5,11,15] In addition to the $T_{\|}$ analysis, a magnetic "beach analyzer" was used to obtain $T_{\perp}$ in one of the experiments. The data show that the two temperatures relax toward a common value, corroborating both measurement techniques. Measurements of $T_{\|}$ were made over the 6 decade range of $3\times 10^{-3}<T_{\|}<300$ eV, with about ±5% accuracy at high temperatures, and ±30% accuracy at low temperatures. At high temperatures the temperature equilibration is as expected from conventional scattering

theory,[11] whereas at low temperatures the equilibration is governed by a many-particle adiabatic invariant.[16]

VI. DISCUSSION

In this section, we consider the limitations of the experimental technique and analysis presented in Sec. III. We conclude that our diagnostic procedure is expected to work best for moderately long plasma columns and for the portion of the distribution function with the highest energy.

The model represented by Eqs. (1)–(3) is based on several assumptions which we here make explicit. In writing Eq. (3), we have ignored the effect of radial variations over the size of the collector. Since the density, plasma potential, confinement potential, and distribution function vary with radius, we should actually perform an integration over the area of the collector. These corrections may be implemented, but they tend to complicate the data analysis. The corrections are of magnitude R_c/ρ where R_c is the collector radius and ρ is a typical scale length for radial variations in n, ϕ_p, ϕ_c, and F. The collector used for Fig. 2 has radius $R_c/R=0.065$, so the variations in Fig. 2 show $R_c/\rho \ll 1$.

Equation (1), and thus Eq. (3), also reflects a simplified model of the axial plasma variation. We assume that the plasma column has flat ends and that the implicit axial integration may be replaced by the column length L. The fall-off of the plasma at the ends of the column actually occurs over some finite distance ΔL, and this distance may vary with radius.[17] However, this leads to corrections in Q_{esc} of the order $\Delta L/L$, which is typically of order λ_D/L or R/L, and is generally small.

Another length-related correction occurs even in the context of the flat-ended column model. The plasma length is the distance between the points where the electrons are reflected by the confining end potentials. This length, however, will increase as the confinement potential approaches zero. While this does not affect the axially integrated charge, it does change the charge per unit length, and thus changes ϕ_p. A separate effect associated with this increase in length is the cooling of $T_\parallel$ due to adiabatic expansion.[11] If we again denote this change in length ΔL, then both of these effects are of order $\Delta L/L$, but in this case ΔL is roughly the same as the scale length of axial variations in ϕ_c, and this scale length is set by the wall radius R (i.e., $\Delta L/L \approx R/L$). This correction may be important for the very short plasmas used in some experiments, but is small for the data shown in Fig. 2 ($R/L=2.5\%$).

A more fundamental limitation of our analysis model is the presumption of no time dependence. It is assumed, for example, that all electrons with the same energy will share the same fate, regardless of the fact that they may be at opposite ends of the plasma column when the dump begins and that some will escape before others. This assumption is justified if the analyzing potential does not change appreciably on the time scale of an electron transit ($L/v_\parallel$) or of an electron plasma wave. Also, the entire measurement must be fast compared to the electron–electron collision time ν_{ee}^{-1}, which is about 5 msec for these plasmas. These conditions can be written

$$\left(\frac{L}{v_\parallel}, \omega_p^{-1}\right) \ll kT_\parallel \left(\frac{dE}{dt}\right)^{-1} \ll \nu_{ee}^{-1}. \tag{9}$$

Note that the first condition is easier to satisfy in a short plasma column than in a long one. However, there are always some particles (the slowest ones) that will not satisfy this condition.

In principle one may satisfy condition (9) by decreasing the rate at which the analysis potential is varied [i.e., by increasing the ramp-up time of the analysis pulse in Fig. 1(b)]. In practice this strategy is limited by the onset of the diocotron instability. As noted above, the electrons at the center of the plasma column (i.e., $r \simeq 0$) are first to escape as the confining potential is made less negative. This leaves the column of confined electrons depleted in the center [see Fig. 2(b)]. It is well known that such hollow electron columns are unstable to diocotron modes.[1,18] As this instability grows, it produces radial transport of electrons.[18] Electrons that move radially inward are then able to escape from the machine. Unless one can dump and measure the escaping charge before the instability grows, the measurement will be confused by transport-related effects.

The problem of diocotron-induced transport is illustrated in Fig. 5. Escaping electrons are collected with the circuit shown in Fig. 5(a). The RC time of the circuit is chosen to be long compared to the time for electrons to escape, but short compared to the machine cycle time. The escaping electrons produce an output voltage change that is proportional to Q_{esc}. Figure 5(b) shows the voltage versus time for several cycles of a typical case. At the first vertical grid line, the confinement potential is ramped to a less negative value and then held at that value. The ramp time is 100 μsec. Electrons having sufficient energy escape and produce the repeatable initial signal, which then begins to decay away with time as charges leak off the collection capacitor. The diocotron instability grows on the remaining hollowed electron column, and moves some electrons radially inward where they can escape from the machine. These electrons produce the voltage changes occurring about 2 divisions (200 μsec) after the first electrons escape. Since the instability grows from noise, these curves are different for each machine cycle.

Figure 5 shows that it is possible in practice to dump and measure the escaping charge before the diocotron instability grows. However, this requires a fast ramp on the analysis pulse and thus a large value of dE/dt, and this requirement conflicts with condition (9). With the minimum value of dE/dt restricted by the instability growth time, and the value of L constrained by the desire to avoid end corrections, condition (9) reduces to a limit on electron velocity. For a given plasma there will always be some electrons that are too slow to satisfy this condition. This explains the failure of the analysis at low energies, as is apparent in Fig. 2(e).

The effects discussed in this section impose some limits on the applicability of this diagnostic, but these limits are not severe. For moderately long plasma columns and typ-

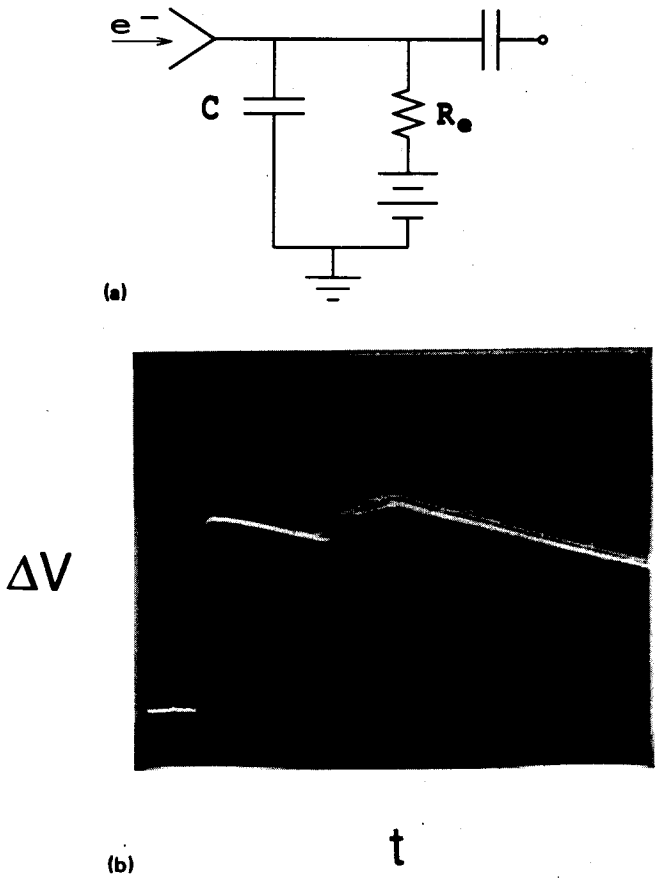

FIG. 5. Dumped electron measurement circuit and typical signal. (a) Circuit used to collect escaping electrons. The initial voltage due to the charge collected on the capacitor is proportional to Q_{esc}, and it decays on a time scale of R_eC. (b) The induced voltage versus time for several plasma dump cycles. The second, nonrepeatable voltage change is due to electrons transported radially by the diocotron instability. Time scale $=100$ μsec/div.

ical collector sizes, the errors encountered are on the order of a few percent, and this is acceptable in most cases. The failure of the technique at low particle energies does not impose a severe restriction, since departures from a Maxwellian distribution usually occur only at higher particle energies.

VII. COMMENTS ON OBTAINING δF IN PERTURBATION EXPERIMENTS

As we have shown, the dependence of Q_{esc} on ϕ_p complicates the interpretation of the Q_{esc} data. However, with proper analysis of these data, one can obtain the parallel electron energy distribution, $F(r,E)$. In many experiments one wishes to find the *change* in F due to some externally applied perturbation which may cause both particle transport and energy transport (i.e., changes in the distribution function). A typical approach would be to apply the perturbation on alternate machine cycles and then measure the *change* in $Q_{esc}(r,\phi_c)$ from cycle to cycle, i.e., $\delta Q_{esc}(r,\phi_c)$. We point out here that the analysis of these data requires special care.

Taking the variation of Eq. (3), we obtain

$$\delta Q_{esc}(r,\phi_c)=\delta Q(r)\int_E^\infty \frac{dE'}{\sqrt{E'}}F(r,E') + Q(r)\int_E^\infty \frac{dE'}{\sqrt{E'}}\delta F(r,E') - Q(r)\frac{F(r,E)}{\sqrt{E}}\delta E. \tag{10}$$

The first term on the right-hand side of Eq. (10) represents the change in Q_{esc} produced by radial transport [i.e., changes in $n(r)$]. The second term is produced by changes in the electron kinetic energies (velocity space transport). The third term is due to changes in the effective analyzer potential, $\phi_c-\phi_p$. The confinement potential ϕ_c is not affected by an applied perturbation, but the plasma potential ϕ_p will change. Thus $\delta E=-q\delta\phi_p$, where $\delta\phi_p$ is obtained from the variation of Eq. (4):

$$\frac{1}{r}\frac{d}{dr}\left(r\frac{d}{dr}\delta\phi_p\right)=\frac{-4\pi}{AL}(\delta Q-\delta Q_{esc}). \tag{11}$$

Here, we have used the relation $Q=nqAL$. Equation (11) may be radially integrated to obtain $\delta\phi_p$, but note that this requires a knowledge of the radial dependence of δQ and δQ_{esc}. In addition, the third term on the right-hand side of Eq. (10) involves F, which is obtained from Q_{esc}. Thus, the data set required to obtain δF in perturbation experiments must include both Q_{esc} and δQ_{esc} as a function of r and ϕ_c.

In some cases one of the terms in Eq. (10) may vanish. For example, if the applied perturbation produces no radial transport, the first term will be zero. Further simplifications, however, are not possible. Either type of transport (configuration space or velocity space) will produce a nonzero value of $\delta\phi_p$, and thus give a nonvanishing third term. Furthermore, the magnitude of this term is typically comparable to the other nonzero term(s), so it cannot be neglected. We conclude that, although perturbation data can be analyzed following Eqs. (10) and (11), there is no simple relation between the measured quantity δQ_{esc} and the change in the distribution function δF.

VIII. CONCLUSIONS

We have presented a technique to measure the parallel energy distribution of particles in a cylindrical pure electron plasma. This technique does not require modification of typical machine geometries, but only a modification of the way the electrons are dumped and analyzed. While a full analysis of the data requires the use of a computer, some information can be obtained using a simplified version of the technique. Both the full and simplified versions of the technique work best for moderately long plasma columns, in which case the uncertainties resulting from the limitations of the analysis model are on the order of a few percent. We have successfully used these techniques in three different experimental contexts.

ACKNOWLEDGMENTS

This work was supported by U.S. Department of Energy Grant No. DEFG 03-85ER53199, National Science Foundation Grant No. PHY87-06358, and Office of Naval Research Grants No. N00014-89-J-1714 and No. N00014-89-J-1399.

[1]See, for example, A. W. Trivelpiece, Comments Plasma Phys. Controlled Fusion **1**, 57 (1972); R. C. Davidson, *Theory of Non-neutral Plasmas* (Benjamin, Reading, MA, 1974); *Non-Neutral Plasma Physics*, edited by C. W. Robertson and C. F. Driscoll (American Institute of Physics, New York, 1988).

[2]J. S. deGrassie and J. H. Malmberg, Phys. Rev. Lett. **39**, 1077 (1977).

[3]J. S. deGrassie and J. H. Malmberg, Phys. Fluids **23**, 63 (1980).

[4]B. R. Beck, Ph.D. dissertation, University of California, San Diego, 1990.

[5]B. R. Beck, J. Fajans, and J. H. Malmberg, Phys. Rev. Lett. **68**, 317 (1992).

[6]J. H. Malmberg and C. F. Driscoll, Phys. Rev. Lett. **44**, 654 (1980); C. F. Driscoll and J. H. Malmberg, Phys. Rev. Lett. **50**, 167 (1983); C. F. Driscoll, K. S. Fine, and J. H. Malmberg, Phys. Fluids **29**, 2015 (1986).

[7]D. L. Eggleston, T. M. O'Neil, and J. H. Malmberg, Phys. Rev. Lett. **53**, 982 (1984).

[8]D. L. Eggleston and J. H. Malmberg, Phys. Rev. Lett. **59**, 1675 (1987).

[9]W. D. White, J. H. Malmberg, and C. F. Driscoll, Phys. Rev. Lett. **49**, 1822 (1982).

[10]T. Hsu and J. H. Hirshfield, Rev. Sci. Instrum. **47**, 236 (1976).

[11]A. W. Hyatt, C. F. Driscoll, and J. H. Malmberg, Phys. Rev. Lett. **59**, 2975 (1987); A. W. Hyatt, Ph.D. dissertation, University of California, San Diego, 1986.

[12]J. H. Malmberg and J. S. deGrassie, Phys. Rev. Lett. **35**, 577 (1975).

[13]A. W. Trivelpiece and R. W. Gould, J. Appl. Phys. **30**, 1784 (1959).

[14]J. H. Malmberg and C. B. Wharton, Phys. Rev. Lett. **17**, 175 (1966).

[15]J. H. Malmberg, C. F. Driscoll, B. Beck, D. L. Eggleston, J. Fajans, K. Fine, X.-P. Huang, and A. W. Hyatt, in *Non-Neutral Plasma Physics*, Ref. 1; B. R. Beck, Bull. Am. Phys. Soc. **33** (1988).

[16]T. M. O'Neil and P. G. Hjorth, Phys. Fluids **28**, 3241 (1985).

[17]A. J. Peurrung and J. Fajans, Phys. Fluids B **2**, 693 (1990).

[18]C. F. Driscoll, Phys. Rev. Lett. **64**, 645 (1990); C. F. Driscoll and K. S. Fine, Phys. Fluids B **2**, 1359 (1990).